Chinese Journal of
POLYMER SCIENCE

RESEARCH ARTICLE

https://doi.org/10.1007/s10118-024-3103-y
Chinese J. Polym. Sci. **2024**, *42*, 886–894

Injection of a Self-propelled Polymer into a Small Circular Cavity

Chao Wang[a*], Yan-Li Zhou[a], Xiao Yang[a], Fan Wu[a], and Meng-Bo Luo[b]

[a] *Department of Physics, Taizhou University, Taizhou 318000, China*
[b] *Department of Physics, Zhejiang University, Hangzhou 310027, China*

Abstract The injection of a polymer chain into a small circular cavity under tangential self-propelled force is studied by using Langevin dynamics simulation. Results indicate that the injection dynamics of the active polymer shows strong correlation with the polymer conformation inside the cavity depending on the polymer rigidity (k_b). The injection time τ varies nonmonotonously with increasing k_b, and reaches its minimum at k_b^*. When k_b is small ($k_b << k_b^*$), the polymer is nearly random coil in the cavity, and spends a long time at the final stage of the injection process due to the large repulsion between monomers inside the cavity. When k_b is moderate ($k_b \sim k_b^*$), the part of polymer inside the cavity forms spiral configuration under the tangential active force, and the whole polymer moves synchronously with a constant velocity during the injection process, leading to a small injection time. When k_b is large ($k_b >> k_b^*$), the polymer is nearly straight at the initial stage of the injection process, and takes a long time to bend itself, leading to a large injection time.

Keywords Active Polymer; Injection; Dynamics; Simulation

Citation: Wang, C.; Zhou, Y. L.; Yang, X.; Wu, F.; Luo, M. B. Injection of a self-propelled polymer into a small circular cavity. *Chinese J. Polym. Sci.* **2024**, *42*, 886–894.

INTRODUCTION

The translocation of polymers through narrow channels from the *cis* space to the *trans* space is related to many biological processes and technological applications, such as transportation of biomacromolecules through channels in biological membranes,[1–4] DNA packaging,[5–8] genome mapping,[9–12] nanochannel-based method for DNA sequencing and separation,[13–19] *etc.*, which is a typical non-equilibrium dynamical process and has attracted lots of attention from the physical, chemical, and biological communities in the last two decades.

Experimentally, the size of the channel is much smaller than that of the polymer in the *cis* space, so successful translocation is often achieved by an external driving mechanism.[18–25] The translocation process is complex, and is influenced by many factors. Theoretically, the dependence of the translocation time (τ) on the polymer length (N) has been extensively studied. For the case that both the *cis* space and the *trans* space are half-infinite, τ as a function of N can be simply expressed as $\tau \propto N^{\alpha}$.[26–28] For the case the *trans* space is a small cavity, the volume exclusive interaction between monomers inside the cavity will produce an effective resistive force on the polymer. It was found that the scaling exponent α is dependent on the driving force (F) and the monomer density (ϕ) in the cavity after the injection, and the dependence of the complete injection time (τ) on F and ϕ can be expressed as $1 - \tau_0/\tau \propto \phi^{\beta}/F$, where τ_0 is the injection time for the extreme case $R \to \infty$ and the scaling exponent β has different values at small and large ϕ.[29–31] The confinement of the cavity not only influences the injection dynamics, but also affects the configuration of the polymer inside the cavity.[32,33] For the flexible polymer, the part of polymer in the capsid maintains a random configuration. While for the semiflexible polymer, the part of polymer in the capsid can form regular structure.

In recent years, the static and dynamical characters of active polymers have been studied extensively. In experiment, the protein motors can exert a tangential active force along the contour of the microtubules or filaments, leading to the activity of microtubules or filaments.[34,35] It was found that polymers with tangential active force behave quite complexly.[36–40] In two-dimensional (2D) space, the active polymer often adopt extended configuration and move along its own contour at weak active force and large bending rigidity, but can spontaneously form stable spiral and undergo rotational motion at strong active force and small bending rigidity.[37] When the active polymer is bonded to a passive load, the polymer can even push or pull the load with different conformational states and motion types.[38–40]

Comparing with free polymers, active polymers under restricted conditions show more complex behaviors. For the head-fixed active polymer in 2D space, the polymer shows spiral form with rotational motion or wave form with flapping motion, depending on the fixed mode of the head.[41–44] For active polymers tethered on an infinite flat surface, the polymer is buckled into a quasi-helical structure with rotational motion at large active force and bending rigidity.[45] For

* Corresponding author, E-mail: chaowang0606@126.com
Received December 30, 2023; Accepted February 10, 2024; Published online March 29, 2024

active polymers adsorbed on the surface of a cylinder, the polymer often forms several typical configurations with specific motion types.[46] For active polymers in a transversal asymmetric channel, the polymer transport direction can be rectified and even show current reversals due to the competition of the polymer chirality and the channel properties.[47] For active polymers in crowded environments, it was found that there is a robust conformational transition, and crowded environments can facilitate polymer diffusion and even separated polymers with different length and activity.[48–50]

Recently, the translocation of active polymers through a pore is studied by several groups. For the case the pore is narrow and short, the polymer behaves a railway motion manner, resulting that the translocation time is independent of the polymer rigidity.[51] While for the case the pore is long, the translocation time shows a nonmonotonic change with increasing pore width owing to the crucial interplay of activity and spatial confinement.[52] Rezaie-Dereshgi *et al*. studied the translocation of an active polymer with fixed rigidity into a circular cavity, and found that the polymer configuration at the end of the translocation for small cavity and large active force is more regular than that for large cavity or small active force.[53] In fact, the polymer rigidity is also a main factor affecting the configuration of the active polymer.[37,45] However, the dependence of the polymer configuration in the cavity and the translocation time on the polymer rigidity is not clear. Motivated by this, the injection of a self-propelled polymer chain into a small circular cavity is studied in this work, and the influence of the polymer rigidity on the configuration and the injection dynamics is mainly investigated. We found that the dependence of the injection time on the polymer rigidity is complex, and the injection dynamics shows remarkable correlation with the polymer configuration in the cavity.

SIMULATION MODELS AND METHODS

Simulation was carried out in the two-dimensional (2D) space, and the geometry of the model system is shown in Fig. 1. A half infinite space (the *cis* side) and a circular cavity (the *trans* side) is connected by a narrow pore. The geometrical boundary of the model system (the wall, the pore and the cavity) is continuous and impenetrable.

In our simulation, the polymer is modelled by a bead-spring chain, in which monomers numbered from 1 (the head) to N (the end) are sequentially connected by elastic bonds. The elasticity of the bond is described by the finitely extensible nonlinear elastic (FENE) potential:

$$U_{\mathrm{FENE}}(r) = -\frac{k}{2}R_0^2 \ln\left[1-\left(\frac{r}{R_0}\right)^2\right] \tag{1}$$

where k is the spring constant, r and R_0 refer the bond length and the maximum bond length, respectively. The volume exclusive interaction between any two monomers is described by the purely repulsive Weeks-Chandler-Andersen (WCA) potential,

$$U_{\mathrm{LJ}}(r) = \begin{cases} 4\varepsilon_0\left[\left(\frac{\sigma}{r}\right)^{12}-\left(\frac{\sigma}{r}\right)^{6}\right]+\varepsilon_0, & r \le r_{\mathrm{cutoff}} \\ 0, & r > r_{\mathrm{cutoff}} \end{cases} \tag{2}$$

where r is the distance between two monomers, ε_0 is the interaction strength, σ is the diameter of monomers, and $r_{\mathrm{cutoff}} = 2^{1/6}\sigma$ is the cut-off distance.

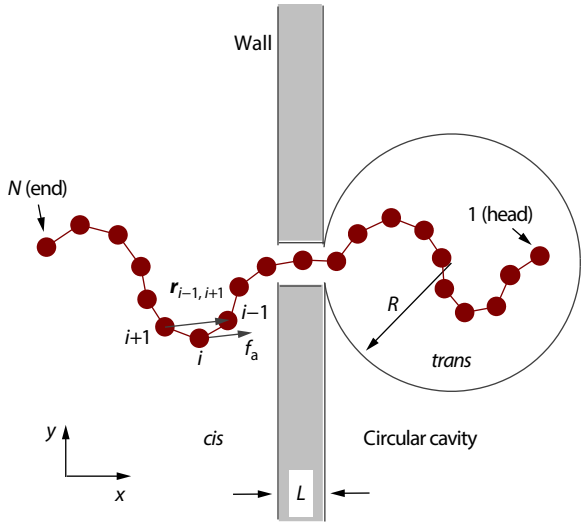

Fig. 1 A sketch of the simulation model system. The *cis* side (a half infinite space) and the *trans* side (a circular cavity with radius R) are connected by a narrow pore with width w_p and length L. The active polymer is composed of N identical beads (monomers), and the ith monomer ($1 < i < N$) is subjected to a tangential force f_a along the vector $r_{i-1,i+1}$ between the position of the monomers i–1 and i+1.

Moreover, to model the rigidity of the polymer chain, the bending energy between two adjacent bonds are also considered, which is described by

$$U_{\mathrm{bend}} = k_b\theta^2 \tag{3}$$

where θ is the angle between two neighboring bond vectors, k_b is the bending rigidity. The polymer becomes more rigid with increasing k_b.

To model the activity of the polymer chain, we assume that the i^{th} monomer is subjected to a self-propelled tangential force,[45,51]

$$\boldsymbol{F}_a^{(i)} = \begin{cases} f_a\dfrac{\boldsymbol{r}_{i-1,i+1}}{|\boldsymbol{r}_{i-1,i+1}|}, & (1 < i < N) \\ 0, & (i = 1 \text{ and } N) \end{cases} \tag{4}$$

where $f_a \ge 0$ represents the strength of the active force, and $\boldsymbol{r}_{i-1,i+1} = \boldsymbol{r}_{i-1} - \boldsymbol{r}_{i+1}$ is the vector between the position of the monomers i–1 and i+1. The polymer is more active with increasing f_a. Under the driving of the active force, the polymer chain can inject into the circular cavity through the pore from the *cis* side.

The interactions between the monomer and the wall, the pore and the circular cavity are also described by the WCA potential (Eq. 1) with r the nearest distance between the monomer and the boundary of the model system.

The motion of each monomer is described by the Langevin equation:

$$m\frac{\mathrm{d}\boldsymbol{v}}{\mathrm{d}t} = -\nabla\left(U_{\mathrm{FENE}} + U_{\mathrm{LJ}} + U_{\mathrm{bend}}\right) + \boldsymbol{F}_a - \eta\boldsymbol{v} + \boldsymbol{F}^{\mathrm{T}} \tag{5}$$

where m is the mass of the monomer, η is the friction coefficient, and $\boldsymbol{F}^{\mathrm{T}}$ is the random force with $<\boldsymbol{F}^{\mathrm{T}}(t)>=0$ and $<\boldsymbol{F}^{\mathrm{T}}(t)\cdot\boldsymbol{F}^{\mathrm{T}}(t')> = 4\eta k_B T\delta(t-t')$, where k_B is the Boltzmann constant and T is the temperature. For the numerical integration of Eq. (5), the velocity Verlet algorithm is adopted with a time step Δt=0.005.

https://doi.org/10.1007/s10118-024-3103-y

At the beginning of the simulation, the polymer is generated in the *cis* side with the head monomer (i=1) being at the middle of the pore. We at first fix the head monomer, and let the simulation run a long time t_s (>10^7) to reach the final steady-state. We then release the head monomer and set this moment as time t=0. Under the driving of the tangential active force, the polymer tries to enter into the cavity. Due to the random thermal fluctuation, the whole polymer may go back to the *cis* side from the pore. In that case, we stop the simulation and begin a new run until the whole polymer injects into the cavity successfully. For the successful injection case, the time interval from the last enter of the head monomer into the cavity to the first enter of the last (N^{th}) monomer into the cavity is defined as the injection time τ. In our work, the results of injection time are averaged over more than 2000 independent samples for each group of the parameters, and the standard deviation is very small.

In this work, σ, m, and k_BT are set as the units of length, mass, and energy, respectively. So, the time scale and the force scale are defined by $t_{LJ} = (m\sigma^2/k_BT)^{1/2}$ and $f_0 = k_BT/\sigma$, respectively. In the simulation, we fix the WCA potential interaction strength ε_0=1, the FENE potential spring constant k=15, the maximum bond length R_0=2, the friction coefficient η=10, and the pore length L=2. Moreover, to ensure the monomer inject into the cavity one by one, we choose a narrow pore with width w_p=2.4. We mainly study the influence of f_a and k_b on the injection time, and uncover the dynamical characters of the injection process.

RESULTS AND DISCUSSION

The Size of the Active Polymer Chain in Free Space

The active force can not only play a role of driving force, but also change the structure of the polymer chain. It was found that the structure of the polymer chain in free space is dependent on the strength of the active force.[37] When f_a is small, the polymer chain often adopts loose random coil conformation. While when f_a is large, the active force can drive the polymer chain to form compacted spiral structure.

To check our model, we have studied the radius of gyration R_g of the active polymer chain in free space. Fig. 2 shows the dependence of R_g on f_a for several different k_b. We can see that R_g for each k_b decreases gradually with increasing f_a, meaning that the active force can decrease the structural size of the polymer chain, which is in agreement with the previous simulation results.[37] Specially, when f_a is large and k_b is small, the polymer chain forms compacted spiral, resulting that R_g for different k_b tends to be a same saturated value at large f_a, as shown in Fig. 2 for k_b=0, 2, and 10 for examples.

The Injection of a Flexible Polymer (k_b=0)

We studied the injection of a flexible polymer under the tangential self-propelled force. Fig. 3 shows the dependence of the injection time τ on the radius of the circular cavity R for different polymer lengths N, where the self-propelled force f_a=0.2, and the bending rigidity k_b=0. When R is small, τ is very large, meaning that the confinement effect of the cavity is strong and it is difficult for the polymer to inject into a small cavity. With the increase of R, τ decreases rapidly, indicating that the confinement effect is weaken remarkably. When R is large, the confinement

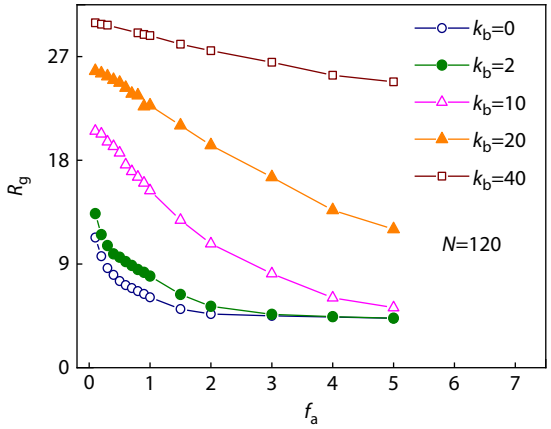

Fig. 2 The dependence of the radius of gyration of polymer in free space R_g on the f_a for five different k_b, where N=120.

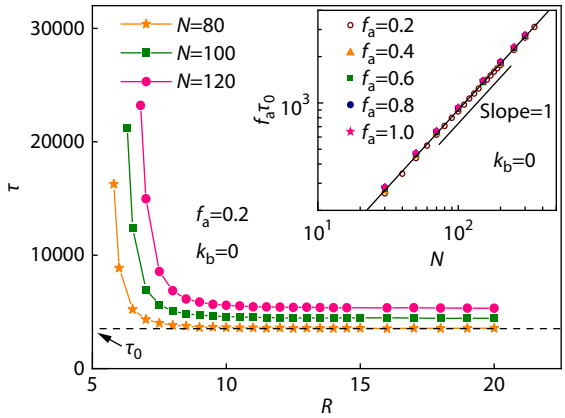

Fig. 3 The dependence of the injection time τ on the radius of the circular cavity R for different polymer length N=80, 100 and 120, where the self-propelled force f_a=0.2, and the bending rigidity k_b=0.

effect is negligible, resulting that τ is nearly independent of R and tends to be an invariable value τ_0. Specially, we calculated the value of τ_0 for different N and f_a at a very large R=1000, and found that the dependence of τ_0 on N and f_a can be described by a simple scaling relation, $\tau_0 \propto N/f_a$, as shown in the inset of Fig. 3, which is the same as the result of the translocation of a self-propelled polymer into a half infinite space.[51]

Qualitatively, during the injection process, the entropy of the polymer decreases and meanwhile the volume exclusive interaction between monomers in the cavity increases gradually, which will produce an effective repulsion to hinder the injection of the polymer. For the injection of a flexible passive polymer under an external driving force F, it was found that the injection time τ can be written by[29,31]

$$\tau = \frac{\tau_0}{1 - f(\phi)/F} \quad \text{or} \quad 1 - \frac{\tau_0}{\tau} = f(\phi)/F \tag{6}$$

where τ_0 is the injection time for the extreme case $R \to \infty$, and $f(\phi)$ represents the average resisting force during the whole injection process, which is a function of the monomer density in the cavity (ϕ) after the injection. For both spherical and circular cavities, it was found that $f(\phi)$ can be expressed as $f(\phi) \propto \phi^{\beta}$, where the exponent β has different values at different ϕ regions.[29,31] Inspired by this, we have studied whether the injection time of a flexible active polymer can also be described by

https://doi.org/10.1007/s10118-024-3103-y

Eq. (6).

Fig. 4 shows the dependence of $1-\tau_0/\tau$ on ϕ for different N at f_a=0.2. In our model, the repulsive interaction between polymer and the wall of the cavity is WCA potential (Eq. 2) with $r_{cutoff}=2^{1/6}\sigma$, and then the distribution of monomers in the cavity with radius R is roughly confined in a circular space with radius $R-r_{cutoff}/2\approx R-0.56$, *i.e.*, the effective radius of the circular is $R_e\approx R-0.56$. Therefore, ϕ is defined as $\phi=N(\pi\sigma^2/4)/(\pi R_e^2)=N\sigma^2/(4R_e^2)$. We can see that the results for different N nearly collapse on a main curve, and $1-\tau_0/\tau$ as a function of ϕ can be expressed as $1-\tau_0/\tau=c\phi^{\delta}$ which is nearly independent of N. Both c and δ are dependent on f_a. Specifically, with f_a increasing, δ increases and saturates gradually, while c decreases monotonously, as shown in the inset of Fig. 4. Specially, c as a function of f_a can be roughly described by $c\propto f_a^{-0.7}$. So, for the injection of a flexible active polymer, we can get

$$1-\frac{\tau_0}{\tau}\propto\phi^{\delta}/f_a^{0.7} \tag{7}$$

From Eqs. (6) and (7), we can roughly obtain the the average resisting force on the polymer, $f\propto f_a^{0.3}\phi^{\delta}$, *i.e.*, the average resisting force depends not only on ϕ but also on f_a, which is different from that of the injection of flexible passive polymers.[29] With f_a increasing, the activity of monomers is strengthened, the collision frequency between monomers and the wall of the circular increases, leading to the increase of the repulsion on the injection process.

The Injection of a Semi-flexible Polymer (k_b>0)

We next studied the injection of a semi-flexible polymer. To enter into the cavity, the polymer has to bend itself, which will cause the increase of the bending energy. Intuitively, it will be more difficult for the polymer to inject into the cavity with k_b increasing. Fig. 5(a) shows the dependence of the injection time τ on the circular radius R for different k_b. For different k_b, τ decreases monotonously with R increasing and tends to be a same saturated value when R is large. At the small R region, it seems that τ for big k_b (=20 and 40) is much smaller than that for small k_b (=2 and 4). Fig. 5(b) shows the dependence of τ on k_b for four small R. For any given small R, τ varies nonmonotonously with k_b increasing, and there is a pronounced valley with minimum injection time τ_{min} at $k_b=k_b^*$ (about 16). This means that a semi-flexible polymer with bending rigidity near k_b^* can inject into small cavities easily. τ_{min} decreases slowly with increasing R, but k_b^* is nearly independent of R. Both τ_{min} and k_b^* are dependent on the active force f_a. Fig. 6 shows the dependence of τ on k_b for different f_a. We can see that the valley is shallower and shallower with f_a increasing, and nearly vanishes when f_a>1. In the region f_a<1, τ_{min} decreases but k_b^* increases monotonously with f_a increasing, as shown in Fig. 6. Based on k_b^*, we can define small k_b (<< k_b^*), moderate k_b (~ k_b^*), and large k_b (>> k_b^*).

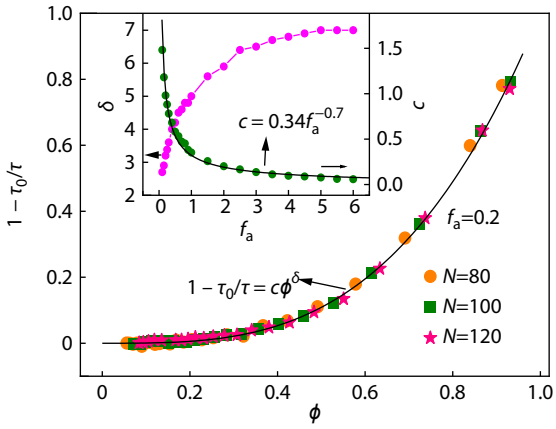

Fig. 4 The dependence of $1-\tau_0/\tau$ on ϕ for N=80, 100, and 120, where f_a=0.2. $1-\tau_0/\tau$ as a function of ϕ can be expressed as $1-\tau_0/\tau=c\phi^{\delta}$. The inset shows the dependence of c and δ on f_a.

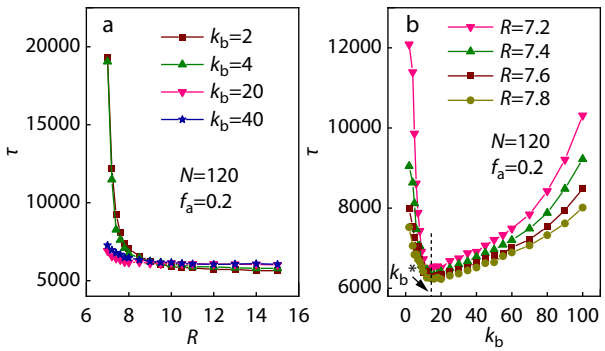

Fig. 5 The dependence of the injection time τ on R for different k_b (a) and on k_b for different R (b). Here, N=120 and f_a=0.2.

To understand the dependence of τ on k_b at small R and small f_a, we have studied the details of the injection process. Fig. 7 shows a series of snapshots of a semi-flexible polymer with k_b=2 (a) and 20 (b) at different time of an injection sample, where N=120, f_a=0.2, and R=7.4. We can see that the configuration of the part of polymer in the cavity is very different for the two k_bs. For k_b=2 (small k_b), it adopts a random coil configuration. While for k_b=20 (big k_b), it forms a spiral configuration.

To show further the conformational property of the polymer in the cavity, we have calculated the tangent-tangent correlation function $C(i)$ of the polymer chain at the end of the injection process, which is defined as[45]

$$C(i)=\frac{\boldsymbol{r}_{1,3}}{|\boldsymbol{r}_{1,3}|}\cdot\frac{\boldsymbol{r}_{i-1,i+1}}{|\boldsymbol{r}_{i-1,i+1}|}\ (1<i<N) \tag{8}$$

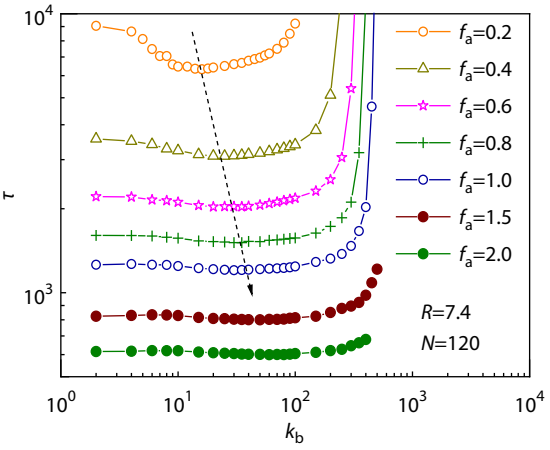

Fig. 6 The dependence of the injection time τ on k_b for different f_a, where R=7.4 and N=120.

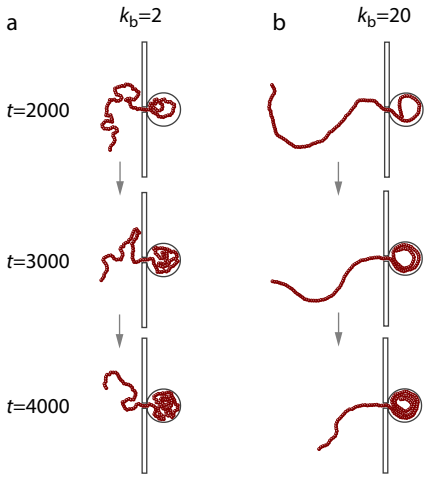

Fig. 7 A series of snapshots of a semi-flexible polymer with k_b=2 (a) and 20 (b) at different time of an injection sample, where N=120, f_a=0.2, and R=7.4.

where $\frac{\boldsymbol{r}_{1,3}}{|\boldsymbol{r}_{1,3}|}$ and $\frac{\boldsymbol{r}_{i-1,i+1}}{|\boldsymbol{r}_{i-1,i+1}|}$ represent the unit tangent vectors at monomers 2 and i, respectively. Fig. 8 presents the dependence of $C(i)$ on i for k_b at N=120, f_a=0.2, and R=7.4. For small k_b (*e.g.*, k_b=2 and 4 in Fig. 8), the configuration of the polymer chain is random coil, and then the correlation between tangent vectors is weak and short-range, *i.e.*, $C(i)$ shows remarkable damping oscillation. While for big k_b (*e.g.*, k_b=20, 30 and 40 in Fig. 8), the configuration of the polymer chain is spiral, and then the correlation between tangent vectors is strong and long-range, *i.e.*, $C(i)$ shows periodical oscillation with nearly constant amplitude.

The nonmonotonous dependence of τ on k_b at small R and small f_a can be qualitatively understood based on the configuration properties of the part of the polymer in the cavity. In the present system, the configuration of the polymer in the cavity depends on the competition between the conformational entropy and the bending energy. Qualitatively, when k_b is small, the conformational entropy dominates, and then the polymer adopts random coil configuration to increase the entropy. In this case, the volume exclusive interaction between monomers inside the cavity will be very strong at the final stage of the injection process, resulting that the polymer has

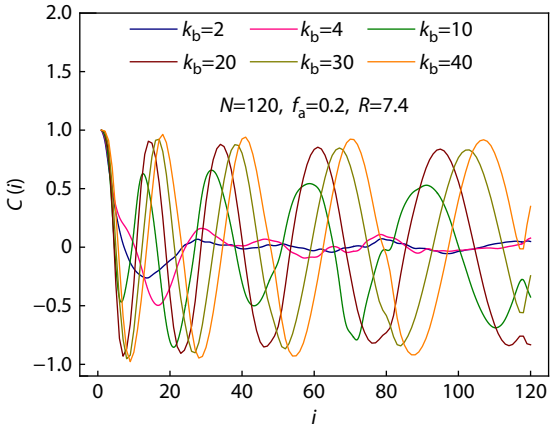

Fig. 8 The tangent-tangent correlation function $C(i)$ for different k_b at N=100, f_a=4, and R=7.4.

to spend a long time to inject into the cavity completely. With k_b increasing, the bend energy dominates gradually. At the early stage of the injection process, the head part of the polymer prefers to bend along the wall of the circular to decrease the bend energy. Under the drive of the tangential self-propelled force, the bend part rolls inward gradually during the injection process, leading to the formation of the spiral configuration. The formation of the spiral configuration in the cavity is beneficial for the injection. On one hand, the spiral configuration can decrease the volume exclusive interaction between monomers in the cavity, and then decrease the repulsion on the polymer. On the other hand, the tangential self-propelled force can drive the spiral part to rotate synchronously during the injection process, as shown in Fig. 7 for k_b=20, which can accelerate further the injection process. Therefore, the injection time decreases with k_b increasing. However, when k_b is large, it is difficult for the polymer to bend itself during the injection process, resulting that the injection time increases with k_b increasing. When is f_a large, the polymer can enter into the cavity quickly, and then the influence of the polymer conformation at small or moderate k_b on the injection dynamics is negligible, leading to the disappearance of the valley on the curve of τ with k_b, as shown in Fig. 6.

For the injection of a semiflexible passive polymer into a cavity driving by an external force in the pore, Zhang *et al.* found that the injection time increases monotonously with k_b increasing,[34] which is quite different from the nonmonotonous dependence of τ on k_b at small R and small f_a for semiflexible active polymer (see Figs. 5b and 6). It was also found that the passive polymer adopts nearly random coil conformation at small k_b and spiral conformation at moderate or large k_b. However, due to the driving force is only in the pore for the passive polymer injection, the spiral part rolls inward passively during the injection process, and can not rotate automatically and synchronously like the the spiral part of the active polymer. Therefore, the formation of the spiral structure of the passive polymer can not quicken the injection process.

To describe the dynamical detail of the injection process at small R and small f_a, we have calculated the residence time t_r which is defined as the duration with m monomers inside the cavity. Fig. 9 shows the dependence of t_r on m for five different k_b, where N=120, f_a=0.2, and R=7.4. We can see that t_r behaves quite differently for small and big k_b. For the case k_b is small (*e.g.*, k_b=2 and 4), t_r is small and nearly independent of m at the early stage of the injection process, because the number of monomers inside the cavity is small and the confinement effect of the cavity is negligible. However, due to the random coil configuration of the polymer inside the cavity, the volume exclusive interaction between monomers is strengthened quickly with m increasing, leading to the quick increase of t_r with m at the final stage of the injection process, as shown in Fig. 9. While for the case k_b is big (*e.g.*, k_b=20, 30 and 40), there are two peaks at the early stage of the injection, which correspond to two trapped stages of the injection process. At small R and big k_b, the part of polymer inside the cavity (the inside part) is nearly linear before the head monomer contacting the wall of the circular. When the head monomer reaches the wall of the cavity, *i.e.*, $m_{p1}l_0 \sim 2R -$

https://doi.org/10.1007/s10118-024-3103-y

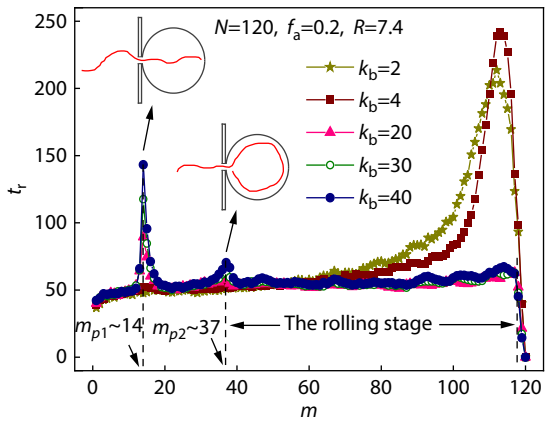

Fig. 9 The dependence of the residence time t_r on the number of monomers m inside the cavity for five different k_b, where N=120, f_a=0.2, and R=7.4.

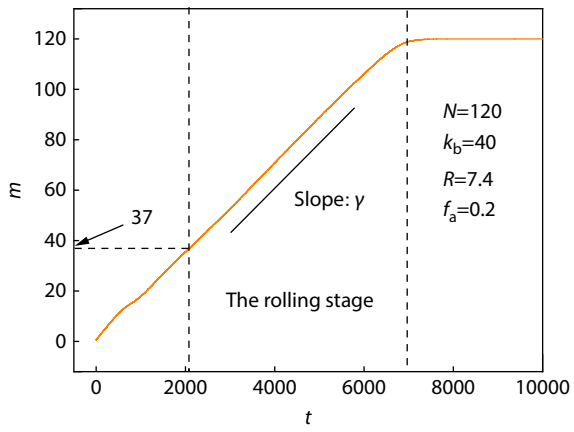

Fig. 10 The evolution of the number of monomers (m) inside the circular cavity at N=120, f_a=0.2, k_b=40, and R=7.4.

r_{cutoff} with l_0 the average bond length, the polymer has to spend a long time to try to bend the inside part, leading to the emergence of the first peak of t_r at $m = m_{p1}$. After the first trapped stage, the inside part of the polymer begins bend along the wall of the circular. When the length of the inside part is about to the circumference of the circular, *i.e.*, $m_{p2}l_0 \sim 2\pi(R - r_{cutoff})$, the head monomer collides with the monomers near the exit of the channel, which will make the polymer spend another long time to try to bend the inside part further, leading to the emergence of the second peak of t_r at $m = m_{p2}$. In our model, the average bond length $l_0 \sim 1$ and $r_{cutoff} \sim 1.12$, and then we have $m_{p1} \sim 14$ and $m_{p2} \sim 39$ for R=7.4, which is in good agreement with our results, as shown in Fig. 9.

Since the two trapped stages are due to the bending attempt of the inside part of the polymer with two special configurations, the sites of the two peaks are independent of k_b, but the value of each peak increases with k_b increasing, as shown in Fig. 9. Moreover, in our model, the active force is exerted on every monomer (except for the two ends monomers), so the effective driving force on polymer increases with f_a or N increasing, resulting that the value of each peak decrease with f_a or N increasing (results not shown). For any given big k_b, the value of the first peak is often bigger than that of the second peak, meaning that it is more difficult for the polymer to bend the straight inside part at m_{p1}.

After the second trapped stage ($m > m_{p2}$), the inside part of the polymer begins a rolling stage, in which the inside part of the polymer forms spiral configuration and rolls inward synchronously during the injection process. Interestingly, t_r is nearly independent of m and k_b when $m > m_{p2}$, as shown in Fig. 9, meaning that the polymer injects into the cavity with a constant velocity and the influence of the bond rigidity on the injection is negligible. To study the velocity of the polymer at the rolling stage, we have counted the number of monomers (m) inside the circular cavity during the injection process.

As an example, Fig. 10 shows the evolution of the number of monomers (m) inside the circular for N=120, k_b=40, f_a=0.2 and R=7.4. For this parameter set, m_{p2}~37 (shown in Fig. 9), and then the polymer is at the rolling stage when 37<m<120. We can see from Fig. 10 that, m nearly increases linearly with t at the rolling stage, *i.e.*, $m = \gamma t$ with γ the slope, indicating that the polymer injects into the cavity with a constant velocity. The velocity of the polymer can be defined as $v = \gamma l_0$, with $l_0 \sim 1$ the average bond length in our model. Fig. 11 presents the dependence of the injection velocity v on f_a for different k_b. Clearly, v increases monotonously with f_a increasing, but is nearly independent of k_b at big f_a. Moreover, when f_a is big, v as a function of f_a can be specifically described by a simple scaling relation $v = 0.1f_a$.

The dependence of v on f_a at large k_b can be understood by the following simple dynamical model. For big k_b, all the monomers of the polymer move nearly synchronously with velocity v at the rolling stage. In a small time interval dt, the energy supplied by the active force, $Nf_a v\mathrm{d}t$, can be roughly divided into two parts. One part is converted into the bond bend energy $\frac{2\pi n k_b}{r} v\mathrm{d}t$ with r the average radius of the spiral part of the polymer and n the number of turns of the spiral, and the other part is dissipated by the work of the viscous force $N\eta v^2\mathrm{d}t$. So, we have $Nf_a v\mathrm{d}t = N\eta v v\mathrm{d}t + \frac{2\pi n k_b}{r} v\mathrm{d}t$, *i.e.*,

$$v = \frac{f_a}{\eta}\left(1 - \frac{2\pi n k_b}{N r f_a}\right) \tag{9}$$

When f_a is big, $\frac{2\pi n k_b}{N r f_a} << 1$, and then we can get from Eq.

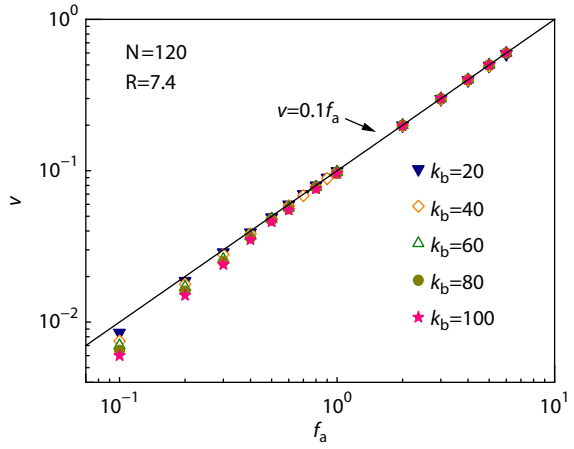

Fig. 11 The dependence of the injection velocity v on f_a for different N, k_b and R.

https://doi.org/10.1007/s10118-024-3103-y

(9) that

$$v \approx \frac{f_a}{\eta} \tag{10}$$

i.e., the velocity v is proportional to f_a, but is nearly independent of k_b. Since η=10 in our simulation, we can get from Eq. (10) that $v \approx 0.1 f_a$, which is in good agreement with the simulation result shown in Fig. 11. While when f_a is small, the second term of Eq. (10) cannot be neglected, so v is smaller than f_a/η and decreases with k_b increasing, as shown in Fig. 11.

We have also investigated the influence of the chain size on the injection dynamics. Fig. 12 shows the dependence of the injection time τ on the polymer length N for different k_b. We can see that the variation of τ with N is dependent on k_b. For large k_b (=30 and 40), τ shows nonmonotonous dependence on N, which can be understood qualitatively by the result of the residence time shown in Fig. 9. When $N < 2R - r_{cutoff}$ (~15 for R=8), the influence of the cavity on the injection process is nearly negligible, and then τ is small and increases with increasing N. While when N>15, the polymer has to be bent to enter into the cavity completely, resulting that the polymer undergoes an obvious trapped stage at $m = m_{p1}$ (~15) during the injection process. At the trapped stage, the total active force F (~$(N-2)f_a$) on the whole polymer tries ceaselessly to bend the polymer. We assume that there are m_t bonds being bent in the cavity at the end of the trapped stage. For N near 15, the total active force F is small, and the trapped time is large, and then the injection process is dominated by the trapped stage. With N increasing, m_t increases gradually, *i.e.*, more and more bonds in the cavity are bent at the end of the trapped stage, leading to the quick increase of τ. We think there must be a specific N, N_s, at which m_t reaches the maximum. For $N > N_s$, with N increasing, the total active force F increases gradually but m_t keeps invariant, resulting that the trapped time as well as τ decrease quickly with N increasing. Therefore, there is a peak on the curve of τ with N at $N = N_s$, as shown in Fig. 12. For given R, the peak is lower and lower with decreasing k_b or increasing f_a, but N_s is nearly independent of k_b and f_a, as shown in Fig. 12 (results are not shown completely). When N>>15, the trapped time is small, and the injection process is dominated by the rolling stage where polymer moves with a constant velocity v, resulting that τ (~Nv) increases with N increasing again. For small k_b (=2, 4 and 10), there is no trapped stage during the injection process. When N is small, the polymer chain can easily enter into the cavity, and τ is small and increases nearly linearly with N increasing. While when N is large, the polymer chain would spend large time at the final stage of the injection process (see Fig. 9), and then and τ is very large and increases quickly with N increasing, as shown in Fig. 12.

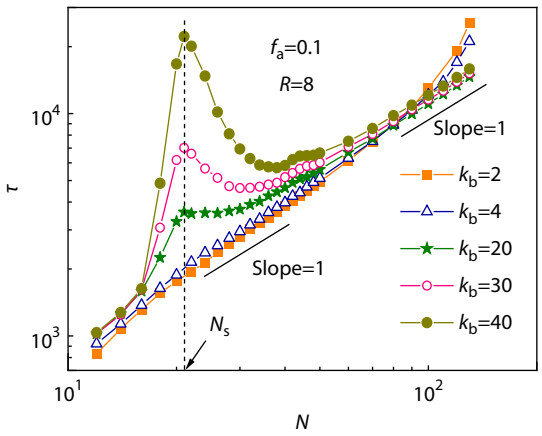

Fig. 12 The dependence of the injection time τ on the polymer length N for different k_b, where f_a=0.1 and R=8.

CONCLUSIONS

In this work, the injection of an active polymer chain into a circular cavity is studied by using Langevin dynamics simulation. The active polymer chain is modelled by a bead-spring chain with each bead subjected to a tangential self-propelled force along the contour of the chain. Due to the confinement of the cavity, the entropy of the polymer decreases and meanwhile the volume exclusive interaction between monomers in the cavity increase gradually during the injection process, which will produce an effective repulsion (f) to hinder the injection. Results show that the self-propelled polymer can enter into the cavity with different configurations and dynamics depending on the polymer rigidity (k_b). The injection time τ varies nonmonotonously with k_b increasing, and reaches its minimum at k_b^*. When k_b is small ($k_b << k_b^*$, including k_b=0), the polymer in the cavity is random coil, and the effective repulsion f is large, resulting that it is difficult for the polymer to inject into the cavity at the final stage of the injection process. Specially, for k_b=0 and any given f_a, the injection time (τ) as a function of the average density of the whole chain in the cavity (ϕ) can be expressed as $1 - \tau_0/\tau = c\phi^{\delta}$ with τ_0 the injection time for infinitely large cavity, which is similar to that of flexible passive polymers. When k_b is moderate ($k_b \sim k_b^*$), the polymer in the cavity can forms spiral configuration quickly under the tangential force, which can decrease the repulsion f and meanwhile make the whole polymer move synchronously, resulting that the polymer can enter into the cavity easily. While when k_b is large ($k_b >> k_b^*$), it is difficult for the polymer to bend itself at the initial stage of the injection process, resulting that it is difficult for the polymer to inject into the cavity again. We also found that τ shows nonmonotonous dependence on N for large k_b and small f_a, and there is a peak on the curve of τ with N, which can be understood qualitatively by the residence time of the injection process.

Finally, although our work was carried out in a 2D system, we would predict that the our simulation results are qualitatively similar to that of a 3D system, since the physics picture governing the injection dynamics are the same for 2D and 3D systems. For both 2D circular or 3D spherical cavity, active polymer would adopt random coil conformation in the cavity when k_b is small, and form rotating spiral when k_b is large. The random coil conformation is disadvantage to the injection process, while the rotating spiral conformation is beneficial to the injection process.

Conflict of Interests

The authors declare no interest conflict.

https://doi.org/10.1007/s10118-024-3103-y

Data Availability Statement

The related data (DOI: 10.57760/sciencedb.j00189.00009) for this study is available in the Science Data Bank database (https://www.scidb.cn/c/cjps).

ACKNOWLEDGMENTS

This work was financially supported by the Zhejiang Provincial Natural Science Foundation of China (No. LY20A040004) and by the National Natural Science Foundation of China (Nos. 11604232 and 11974305).

REFERENCES

1 Laemmli, U. K.; Favre, M. Maturation of the head of bacteriophage T4: I. DNA packaging events. *J. Mol. Biol.* **1973**, *80*, 575–599.
2 Simon, S. M.; Blobe, G. A protein-conducting channel in the endoplasmic reticulum. *Cell* **1991**, *65*, 371–380.
3 Gabashvili, I. S.; Gregory, S. T.; Valle, M.; Grassucci, R.; Worbs, M.; Wahl, M. C.; Dahlberg, A. E.; Frank, J. The polypeptide tunnel system in the ribosome and its gating in erythromycin resistance mutants of L4 and L22. *Mol. Cell* **2001**, *8*, 181–188.
4 Helenius, J.; Ng D. T. W.; Marolda, C. L.; Walter, P.; Valvano, M. A.; Aebi, M. Translocation of lipid-linked oligosaccharides across the ER membrane requires Rft1 protein. *Nature* **2002**, *415*, 447–450.
5 Smith, D. E.; Tans, S. J.; Smith, S. B.; Grimes, S.; Anderson, D. L.; Bustamante, C. The bacteriophage ϕ29 portal motor can package DNA against a large internal force. *Nature* **2001**, *413*, 748.
6 Fuller, D. N.; Raymer, D. M.; Kottadiel, V. I.; Rao, V. B.; Smith, D. E. Single phage T4 DNA packaging motors exhibit large force generation, high velocity, and dynamic variability. *Proc. Natl. Acad. Sci. U. S. A.* **2007**, *104*, 16868–16873.
7 Fuller, D. N.; Raymer, D. M.; Rickgauer, J. P.; Robertson, R. M.; Catalano, C. E.; Anderson, D. L.; Grimes, S.; Smith, D. E. Measurements of single DNA molecule packaging dynamics in bacteriophage λ reveal high forces, high motor processivity, and capsid transformations. *J. Mol. Biol.* **2007**, *373*, 1113–1122.
8 Rickgauer, J. P.; Fuller, D. N.; Grimes, S.; Jardine, P. J.; Anderson, D. L.; Smith, D. E. Portal motor velocity and internal force resisting viral DNA packaging in bacteriophage ϕ29. *Biophys. J.* **2008**, *94*, 159–167.
9 Levy, S. L.; Craighead, H. G. DNA manipulation, sorting, and mapping in nanofluidic systems. *Chem. Soc. Rev*. **2010**, *39*, 1133-1152.
10 Lam, E. T.; Hastie, A.; Lin, C.; Ehrlich, D.; Das, S. K.; Austin, M. D.; Deshpande, P.; Cao, H.; Nagarajan, N.; Xiao, M.; Kwok, P. Y. Genome mapping on nanochannel arrays for structural variation analysis and sequence assembly. *Nat. Biotechnol.* **2012**, *30*, 771–776.
11 Sriram, K. K.; Yeh, J. W.; Lin, Y. L.; Chang, Y. R.; Chou, C. F. Direct optical mapping of transcription factor binding sites on field-stretched λ-DNA in nanofluidic devices. *Nucleic Acids Res.* **2014**, *42*, e85.
12 Lacroix, J.; Pélofy, S.; Blatché, C.; Pillaire, M. J.; Huet, S.; Chapuis, C.; Hoffmann, J. S.; Bancaud, A. Analysis of DNA replication by optical mapping in nanochannels. *Small* **2016**, *12*, 5963-5970.
13 Yuan, Z. S.; Liu, Y. M.; Dai, M.; Yi, X.; Wang, C. Y. Controlling DNA translocation through solid-state nanopores. *Nanoscale Res. Lett.* **2020**, *15*, 80.
14 Wang, C.; Zhou, Y. L.; Sun, L. Z.; Chen, Y. C.; Luo, M. B. Simulation study on the migration of diblock copolymers in periodically patterned slits. *J. Chem. Phys.* **2019**, *150*, 164904.
15 Luo, K.; Ala-Nissila, T.; Ying, S.; Bhattacharya, A. Sequence dependence of DNA translocation through a nanopore. *Phys. Rev. Lett.* **2008**, *100*, 058101.
16 Wang, C.; Chen, Y. C.; Zhang, S.; Luo, M. B. Translocation of diblock copolymer through compound channels: a Monte Carlo simulation study. *Macromolecules* **2014**, *47*, 7215–7220.
17 Magill, M.; Falconer, C.; Waller, E.; de Haan, H. W. Translocation time through a nonopore with an internal cavity is minimal for polymers of intermediate length. *Phys. Rev. Lett.* **2016**, *117*, 247802.
18 Han, J.; Craighead, H. G. Separation of long DNA molecules in a microfabricated entropic trap array. *Science* **2000**, *288*, 1026–1029.
19 Kasianowicz, J. J.; Brandin, E.; Branton, D.; Deamer, D. W. Characterization of individual polynucleotide molecules using a membrane channel. *Proc. Natl. Acad. Sci. U. S. A.* **1996**, *93*, 13770–13773.
20 Bhattacharya A, S. S. Tug of war in a double-nanopore system. *Phys. Rev. E* **2020**, *101*, 052407.
21 Ding, M.; Duan, X.; Lu, Y.; Shi, T. Flow-induced ring polymer translocation through nanopores. *Macromolecules* **2015**, *48*, 6002–6007.
22 Li, X.; Pivkin, I. V.; Liang, H. Hydrodynamic effects on flow-induced polymer translocation through a microfluidic channel. *Polymer* **2013**, *54*, 4309–4317.
23 Keyser, U. F.; Koeleman, B. N.; Dorp, S. V.; Krapf, D.; Smeets, R. M. M.; Lemay, S. G.; Dekker, N. H.; Dekker, C. Direct force measurements on DNA in a solid-state nanopore. *Nat. Phys.* **2006**, *2*, 473–477.
24 Peng, H. B.; Ling, X. S. Reverse DNA translocation through a solid-state nanopore by magnetic tweezers. *Nanotechnology* **2009**, *20*, 185101.
25 Nelson, E. M.; Li, H.; Timp, G. Direct, concurrent measurements of the forces and currents affecting DNA in a nanopore with comparable topography. *ACS Nano* **2014**, *8*, 5484–5493.
26 Sakaue, T. Nonequilibrium dynamics of polymer translocation and straightening. *Phys. Rev. E* **2007**, *76*, 021803.
27 Dubbeldam, J. L. A.; Rostiashvili, V. G.; Milchev, A.; Vilgis, T. A. Forced translocation of a polymer: dynamical scaling versus molecular dynamics simulation. *Phys. Rev. E* **2012**, *85*, 041801.
28 Luo, M. B.; Cao, W. P. Influence of polymer-pore interaction on the translocation of a polymer through a nanopore. *Phys. Rev. E* **2012**, *86*, 031914.
29 Zhang, K. H.; Luo, K. F. Dynamics of polymer translocation into a circular nanocontainer through a nanopore. *J. Chem. Phys.* **2012**, *136*, 185103.
30 Wang, C.; Wu, F.; Zhao, B.; Chen, Y. C.; Luo, M. B. Spontaneous injection of polymer into a spherical cavity from a narrow tube. *Macromolecules* **2020**, *53*, 1694–1700.
31 Wang, C.; Wu, F.; Yang, X.; Chen, Y. C.; Luo, M. B. Driven injection of a polymer into a spherical cavity: a Langevin dynamics simulation study. *Chin. Phys. B* **2021**, *30*, 108202.
32 Ali, I.; Marenduzzo, D.; Yeomans, J. M. Dynamics of polymer packaging. *J. Chem. Phys.* **2004**, *121*, 8635–8641.
33 Zhang, K. H.; Luo, K. F. Polymer translocation into a confined space: influence of the chain stiffness and the shape of the confinement. *J. Chem. Phys.* **2014**, *140*, 094902.
34 Kron, S. J.; Spudich, J. A. Fluorescent actin filaments move on myosin fixed to a glass surface. *Proc. Natl. Acad. Sci. U. S. A.* **1986**, *83*, 6272–6276.
35 Liu, L.; Tüzel, E.; Ross, J. L. Loop formation of microtubules during gliding at high density. *J. Phys.: Condens. Matter* **2011**, *23*, 374104.
36 Bianco, V.; Locatelli, E.; Malgaretti, P. Globulelike conformation and enhanced diffusion of active polymers. *Phys. Rev. Lett.* **2018**,

121, 217802.
37 Isele-Holder, R. E.; Elgeti, J.; Gompper, G. Self-propelled worm-like filaments: spontaneous spiral formation, structure, and dynamics. *Soft Matter* **2015**, *11*, 7181–7190.
38 Isele-Holder, R. E.; Jäger, J.; Saggiorato, G.; Elgeti, J.; Gompper, G. Dynamics of self-propelled filaments pushing aload. *Soft Matter* **2016**, *12*, 8495–8505.
39 Chelakkot, R.; Gopinath, A.; Mahadevan, L.; Hagan, M. F. Flagellar dynamics of a connected chain of active, polar, Brownian particles. *J. R. Soc. Interface* **2014**, *11*, 20130884.
40 Hu, H. X.; Shen, Y. F.; Wang, C.; Luo, M. B. Dynamics of a two-Dimensional active polymer chain with a rotation-restricted active head. *Soft Matter* **2022**, *18*, 8820–8829.
41 Fily, Y.; Subramanian, P.; Schneider, T. M.; Chelakkot, R.; Gopinath, A. Buckling instabilities and spatio-temporal dynamics of active elastic filaments. *J. R. Soc. Interface* **2020**, *17*, 20190794.
42 Sekimoto, K.; Mori, N.; Tawada, K.; Toyoshima, Y. Y. Symmetry breaking instabihties of an *in vitro* biological system. *Phys. Rev. Lett.* **1995**, *75*, 172–175.
43 Bourdieu, L.; Duke, T.; Elowitz, M. B.; Winkelmann, D. A.; Leibler, S.; Libchabe, A. Spiral defects in motility assays: a measure of motor protein force. *Phys. Rev. Lett.* **1995**, *75*, 176–179.
44 Laskar, A.; Singh, R.; Ghose, S.; Jayaraman, G.; Kumar, P. B. S.; Adhikari, R. Hydrodynamic instabilities provide a generic route to spontaneous biomimetic oscillations in hemomechanically active filaments. *Sci. Rep.* **2013**, *3*, 1964.
45 Wang, C.; Zhou, Y. L.; Yang, X.; Chen, Y. C.; Shen, Y. F.; Luo, M. B. Conformation and dynamics of a tethered active polymer chain. *Phys. Rev. E* **2022**, *106*, 054501.
46 Shen, C.; Qin, C. R.; Xu, T. L.; Chen, K.; Tian, W. D. Structure and dynamics of an active polymer adsorbed on the surface of a cylinder. *Soft Matter* **2022**, *18*, 1489–1497.
47 Xu, G. H.; Li, F. G.; Wu, J. C.; Ai, B. Q. Rectification of an active polymer chain with chirality in a transversal asymmetric channel. *Physica A* **2021**, *575*, 126051.
48 Yan, R.; Tan, F.; Wang, J. L.; Zhao, N. R. Conformation and dynamics of an active filament in crowded media. *J. Chem. Phys.* **2023**, *158*, 114905.
49 Wu, S.; Li, J. X.; Lei, Q. L. Facilitated dynamics of an active polymer in 2D crowded environments with obstacles. *Soft Matter* **2022**, *18*, 9263–9272.
50 Heeremans, T.; Deblais, A.; Bonn, D.; Woutersen, S. Chromatographic separation of active polymer-like worm mixtures by contour length and activity. *Sci. Adv.* **2022**, *8*, eabj7918.
51 Wang, C.; Hu, H. X.; Zhou, Y. L.; Zhao, B.; Luo, M. B. Translocation of a self-propelled polymer through a narrow pore. *Chinese J. Polym. Sci.* **2022**, *40*, 1670–1678.
52 Tan, F.; Yan, R.; Zhao, C. N.; Zhao, N. R. Translocation dynamics of an active filament through a long-length scale channel. *J. Phys. Chem. B* **2023**, *127*, 8603–8615.
53 Rezaie-Dereshgi, A.; Khalilian, H.; Sarabadani, J. Translocation of an active polymer into a two dimensional circular nano-container. *J. Phys.: Condens. Matter* **2023**, *35*, 355101.

https://doi.org/10.1007/s10118-024-3103-y